Precise measurements of positron-helium total cross sections from 0.6 to 22 eV

T. Mizogawa, Y. Nakayama, T. Kawaratani, and M. Tosaki*
Institute for Chemical Research, Kyoto University, Sakyo-ku, Kyoto 606, Japan
(Received 6 August 1984)

New precise measurements for positron-helium absolute total cross sections have been performed over the energy range from 0.6 to 22 eV. A high-resolution time-of-flight spectrometer with a straight flight tube and weak axial magnetic field was designed to achieve effective reduction of forward-scattering errors. Observed results around the Ramsauer-Townsend minimum are close to the theoretical results by Campeanu and Humberston, and the remaining slight discrepancies are fully explained by taking account of incomplete discrimination against forward scattering. The results for the energy region excluding the vicinity of the minimum have been obtained with a few percent overall errors, and they are in excellent agreement with some theoretical results. The sources of systematic errors associated with the use of an axial magnetic field are clearly assessed.

I. INTRODUCTION

Since the pioneering work of Costello *et al.*,[1] much experimental effort has been devoted to the study of low-energy positron-helium collisions,[2] for it is the first stage for testing experimental and theoretical methods to study positron-atom collisions. The total cross section (TCS) is of special importance because it can be absolutely measured with comparative ease and higher accuracy than the differential or partial cross sections, and can be used as a reference value for normalizing the cross sections obtained in "relative" measurements.

Many results of measurements for positron-helium TCS's now exist, covering the energy range from 0.3 to 1000 eV. Several recent results are in reasonable agreement with one another over the major portion of the measured energy range. Discrepancies of several tens of percent, however, still exist among the results of different groups for the energy range of a few eV, where the Ramsauer-Townsend minimum occurs. The TCS's reported by Stein *et al.*[3] are about 20% lower than those of Canter *et al.*[4] around 2 eV. The results of Burciaga *et al.*[5] are lower than those of Stein *et al.* in the same energy region. The TCS's of Canter *et al.* are in better agreement with the results of the elaborate theoretical calculation by the Kohn variational method[6,7] than the others in this energy region, although above 3.5 eV there are indications of inconsistencies[8,9] of the Canter *et al.* results with the theoretical values. Humberston[10] pointed out the possible underestimate in the results of Stein *et al.* and Burciaga *et al.* due to insufficient discrimination against forward-scattered positrons, which tends to be more serious near the Ramsauer-Townsend minimum. His argument seems to be convincing.

The results of Canter *et al.*, however, do not cover the energy range below 2 eV, and have failed to reveal the Ramsauer-Townsend minimum directly, while the results of Stein *et al.* are the first direct observation of the minimum. The other previous observation of the minimum has been made by Wilson.[11] His results (corrected by Sinapius *et al.*[12]) are in good agreement with the theory quoted above, as expected from the small discrimination angle (7°) for forward scattering.[12] Their absolute determination of TCS's,[12] however, contains a large systematic uncertainty of 8%, and their more definite results are deduced from the measured ratios of positron TCS's to electron TCS's by normalizing them to the literature values of electron absolute TCS's. Furthermore, the narrow measured energy range, from 1 to 6 eV, makes it difficult to examine their results using the TCS's in the higher energy region, where the agreement between the measurements of different groups is better than the lower-energy region.

Considering the situation mentioned above, new absolute measurements over the wider energy range with adequate consideration of the forward-scattering discrimination should help to resolve the ambiguity in the vicinity of the Ramsauer-Townsend minimum and to establish reliable experimental TCS's in low-energy positron-helium scattering. In the present work, we measured the TCS of positron-helium in the energy region from 0.6 to 22 eV, using an improved transmission method with high-resolution time-of-flight (TOF) energy determination.

The experimental apparatus and the experimental procedure and methods of data analysis are described in Secs. II and III, respectively. Experimental errors are fully discussed in Sec. IV. Finally, in Sec. V the results are presented and compared to several previously existing experimental and theoretical results.

II. APPARATUS

The schematic diagram of the TOF spectrometer with details of the slow-positron source assembly is shown in Fig. 1. A solenoid coil consisting of three parts was wound around the vacuum chamber so that it produces an almost uniform axial magnetic field over the whole flight path, in order to increase the transmission of slow positrons by guiding them along the axial field. Such a guiding field has been often employed by previous experimental groups,[3–5] in order to make the experiments practicable with relatively low intensity incident beams. It can cause, however, two kinds of systematic errors which be-

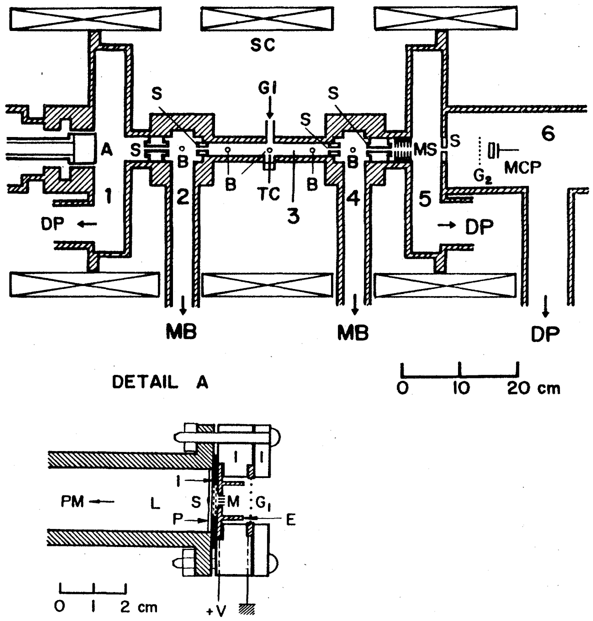

FIG. 1. Schematic diagram of TOF spectrometer. *A*, source-moderator assembly (see detail *A*: PM, photomultiplier tube; *L*, light pipe; *S*, ^{22}Na source; *P*, 0.4-mm-thick plastic scintillator of which moderator side is covered with aluminized Mylar for light reflection. The aluminized surface is in contact with the moderator; *I*, insulators; *M*, moderator consisting of tungsten ribbons and meshes; *E*, copper electrode; G_1, grounded grid); *S*, 4-mm-diam cylindrical apertures; *B*, pressure-gauge ports (for Baratron 310BHS); TC, thermocouple; GI, gas inlet; MS, multislit; G_2, grounded grid; MCP, micro-channel-plate detector; DP, oil diffusion pump with water-cooled baffle; MB, mechanical booster pump with liquid-nitrogen-cooled oil trap; SC, solenoid coil consisting of three parts. The numbers 1–6 are the region numbers (see Sec. II).

come significant in a low-energy region. One is the underestimate of TCS's due to incomplete discrimination against forward scattering and the other is the overestimate of TCS's due to the increase of positron path length in the gas cell by spiraling. It should be noted that both effects become small as the field strength becomes weak, or as the geometrically allowed spiraling radius becomes small. Therefore our actual choice is to weaken the field strength as far as the loss of incident beam is tolerable. The present spectrometer was designed along these lines, and is characterized by a straight flight tube, a localized gas cell, a weak magnetic field, and a small-radius cylindrical-aperture system which confines paths of incident and scattered positrons close to the spectrometer axis. Furthermore, the uniformity of the magnetic field makes quantitative evaluation of the errors mentioned above quite simple, as discussed in Sec. IV.

About 90 μCi of ^{22}Na was mounted between a light pipe and a plastic-scintillator disk of 2 cm diameter and 0.4 mm thickness. The scintillator provides one timing signal for TOF measurements when a fast positron from the source penetrates the scintillator with a partial loss of its energy. The fast positron then impinges on a moderator consisting of tungsten ribbons and meshes. A slow positron, reemitted from the moderator and accelerated to a desired energy, is transported through five 4-mm-diam cylindrical apertures along the axis of the straight flight tube, and finally detected by a micro-channel-plate detector (MCP) which provides the other timing signal. The signals from the scintillator and MCP are fed via constant-fraction discriminators into the stop and start inputs of a time-to-amplitude convertor (TAC), respectively, and the output pulses of the TAC are accumulated in a multichannel pulse-height analyzer. Overall time resolution of the system, 1.2 nsec, was achieved by employing the thicker scintillator than the other groups and the MCP which has excellent timing properties.

Helium gas of 99.999% or 99.9999% purity is introduced at the center of the gas cell via a double molecular-sieve trap cooled by liquid nitrogen to remove possible residual impurities and to reduce outgassing from the inner surface of the piping. The flowing helium gas is pumped out from both sides of the gas cell by a mechanical booster pump with a liquid-nitrogen-cooled trap.

The apertures divide the flight tube into six regions (numbered 1–6, see Fig. 1). Gas pressure can be measured with a precision capacitance manometer (Baratron 310BHS) at one of five ports located at the regions 2, 3, and 4, and with three ionization gauges at the regions 1, 2, and 6. No significant pressure difference was observed among three ports in region 3. Gas pressures of the regions 2 and 4 show the same value, and the ratio of them to the pressure in region 3 increases from $\frac{1}{7}$ to $\frac{1}{6}$ as the pressure of region 3 decreases from 0.12 to 0.04 Torr, where the actual measurements were performed. As this ratio was stable enough, only the pressure in region 3 was continuously monitored during the actual measurements. The gas flow was automatically controlled through a piezoelectric valve to keep the pressure constant. Throughout the measurements the deviation of manometer readings from the pressure setting was less than 1×10^{-4} Torr. The pressures in regions 1 and 6 were less than 1×10^{-5} and 3×10^{-6} Torr, respectively, and not significantly affected by introduction of the gas.

Gas temperature is assumed to be the same as that of the gas-cell wall, which was continuously measured with a thermocouple at the center of region 3 and recorded by a precision pen-recorder.

Since the solenoid field should be weak to reduce the errors, as discussed before, close attention was paid to reducing the earth's and unexpected stray magnetic fields. The axis of the apparatus was directed approximately parallel to the magnetic meridian line. Vertical and east-west components of the earth's magnetic field were canceled by using a double-pair-circular-type Helmholtz coil and a single-pair-square-type Helmholtz coil,[13] respectively. Actually, the currents of these coils were adjusted so as to get the maximum positron transmission. The whole flight tube was constructed with 316 stainless steel, which was annealed after machining for demagnetization. All vacuum pumps, made of iron, were located at least 2 m from the flight tube. Consequently, the residual stray magnetic field was estimated to be less than 10 mG over the whole flight path. The obtained intensity of the slow positron beam was about 0.4/sec in a 13-G solenoid field.

The distance between the moderator and the first grounded grid G_1 is 1 cm, and that between G_1 and the second grounded grid G_2 in front of the MCP is 66 cm. The kinetic energy of a positron is determined from these lengths and the measured flight time on the basis of the following assumptions: the acceleration is constant between the moderator and the grid G_1; the velocity is constant between the two grounded grids; the elapsed time between the light flashing in the scintillator due to the fast positron penetration and the reemission of the slow positron from the moderator is negligible. On these assumptions a flight time uniquely corresponds to a kinetic energy for a fixed acceleration voltage, even though the slow positrons emitted from the moderator have some energy distribution inherently. An overall check of this energy determination was performed for two different energy regions by the observation of two well-known electron resonances using secondary electrons ejected from the moderator by the impinging fast positrons. This was performed by measuring the energy dependence of electron TCS's. Precise absolute determinations of TCS's for electrons were not made, mainly because of the difficulty of gas handling at the required pressures, which are much lower than for the positron case. For the lower-energy region the electron-nitrogen resonance in the vicinity of 2 eV was used. The results are shown in Fig. 2. The location of the fine structure of the resonance differs from Kennerly's results[14] by no more than a few tens of meV. For the higher-energy region the electron-helium resonance, of which the exact location reported by Cvejanovic and Read[15] is 19.361±0.009 eV, was used. The results are shown in Fig. 3. The observed location of the center of the resonance is 19.2 eV. This slight discrepancy can be explained by assuming a 0.5% error of time calibration or a 1 nsec error of the flight-time measurement. The accuracy of the energy determination is, however, acceptable for the present purpose, and it can be concluded that various possible error sources (contact potential differences, charging of the insulators, and so on) are not significant at these energies.

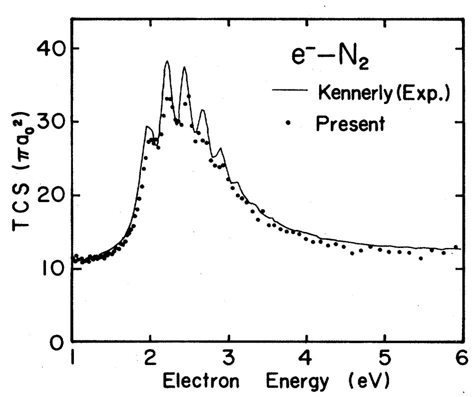

FIG. 2. Measured energy dependence of electron-nitrogen total cross sections around the resonance at a few eV. The present values are normalized to Kennerly's absolute results of Ref. 14 at 1 eV. Axial magnetic field of 6.5 G was applied.

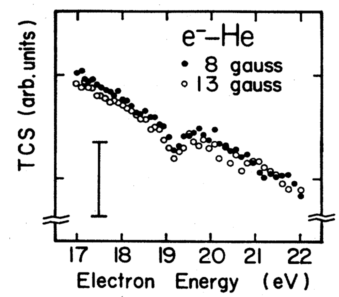

FIG. 3. Measured energy dependence of electron-helium total cross sections around the resonance at 19.36 eV. Vertical scale is indicated by a bar representing 10% of TCS.

III. PROCEDURE AND ANALYSIS

The present experimental conditions to measure positron-helium TCS's are tabulated in Table I. The energy range from 0.6 to 22 eV was covered, and for some energy regions several independent measurements under different experimental conditions were performed in order to examine unexpected systematic errors.

The TCS's, denoted as σ, are determined from the equation

$$\sigma=\left[\int \rho(l)dl\right]^{-1}\ln(n_v/n_g)\ , \tag{1}$$

where n_v and n_g are the count rates of positrons fallen into the corresponding energy bins of the "vacuum" and "gas" spectra, respectively. The number density of helium atoms at a point l on the flight path in denoted as $\rho(l)$. The integration is taken over the whole flight path.

A "run" consists of measurements of three spectra, i.e., vacuum, gas, and "calibration" for random coincidence correction.[16] Extremely long accumulation time is required for each run because of the weakness of the incident beam, and may possibly introduce appreciable variation of the beam intensity during the run. In order to minimize the error due to the change in beam intensity, each run (except for the calibration measurement) was divided into 8–16 short "segments." Each segment consists of two alternate periods for vacuum and gas spectra. A typical length of a segment was a day or half a day, and

TABLE I. Experimental conditions.

Axial magnetic field strength[a] (G)	Acceleration voltage (V)	Gas pressure[b] (Torr)
8	−0.5, 0.5	0.12
13	−1.0, 0, 1.0, 3.0	0.12
13	3.0, 4.0, 7.0, 10.0, 13.0, 15.0, 17.0, 18.5, 20.0	0.06
8	15.0, 16.5, 18.5, 19.5	0.06
8	19.5	0.04

[a]Measured at the cylindrical aperture in front of the MCP.
[b]Measured at region 3 (see Sec. II).

the sharing ratio of time between vacuum and gas was typically 1:2. After the whole measurements of a run, the value $\ln(N_v/N_g)$, where N_v and N_g are the numbers of detected slow positrons during the vacuum and gas period, respectively, was calculated for each segment in order to check the effect of the intensity drift. When the standard deviation of the values throughout the run was much larger than expected statistically, then the whole set of data of the run were discarded.

Since the decay of the ^{22}Na source during several runs is not negligibly small, a "calibration spectrum" for random coincidence correction was measured at the middle of each run, with 60-Hz regular pulses as start signals and photomultiplier pulses as stop signals for the TAC. The vacuum and gas spectra summed over all the segments in the run are processed with the "signal restoration" procedure,[16] by using the calibration data.

The "restored" TOF spectra are then converted to energy spectra with constant bin width (0.5 eV for such runs as measured with 13-G solenoid field and the accelerating voltages higher than 3 V, and 0.2 eV for the others). The TCS for each energy bin is deduced from the energy spectra by the use of Eq. (1). Since the slow positron peak in each spectrum has about 2 eV width, TCS's within this width can be determined simultaneously.

The integral $\int \rho(l)dl$ in Eq. (1) is evaluated as follows:

$$\int \rho(l)dl=(k_BT)^{-1}\int P(l)dl=(k_BT)^{-1}(l_1P_1+l_2P_2)\ , \quad (2)$$

where k_B is the Boltzmann constant, T is the mean temperature of gas during the run, and $P(l)$ is the pressure at the point l. P_1 and P_2 are the pressures in the region 3 and 2 (or 4), respectively, and l_1 and l_2 are the effective lengths of the regions where the pressures are P_1 and P_2, respectively. Pressure gradients in the cylindrical apertures are assumed simply to be constant (see Fig. 4). On this assumption l_1 and l_2 are evaluated as $l_1=22$ cm and $l_2=14$ cm. Since P_1 is 6 or 7 times as large as P_2, the contribution of l_2P_2 to the integral $\int P(l)dl$ is less than 10%.

A thermal transpiration correction to the measured pressure is necessary to obtain the real pressure P_1 because of the difference between the temperatures of the manometer sensor head (regulated at 45 °C; denoted as T') and the gas cell (around 25 °C; denoted T). (The correction for P_2 has no significant effect on TCS.) Because of relatively high pressure in region 3, the Liang equation

$$\frac{P_1}{P_1'}=\frac{R_m+\alpha DP_1'+\beta(DP_1')^2}{1+\alpha DP_1'+\beta(DP_1')^2} \quad (3)$$

was used with the constants α and β given by Edmonds and Hobson,[17] where P_1' is the measured pressure and P_1 is the true pressure in the region 3. The parameter D was taken to be 6 mm, the same as the tube diameter near the sensor. The low-pressure limit of the correction factor, R_m, for a capacitance manometer was reported[14,18] to be considerably different from the theoretical value $(T/T')^{1/2}$. Since in the present work we have no means to measure R_m directly, we adopted an average of "full" and "no" correction

$$R_m=\tfrac{1}{2}(1+\sqrt{T/T'})\ , \quad (4)$$

as a tentative choice. There is of course no evidence to support this choice, although Eq. (4) gives approximately the same value of R_m as previously reported. A systematic error in TCS's may be caused by this choice, and in the worst case it might amount to the same order of magnitude as the correction itself. The resultant correction to the TCS is, however, no more than 0.8%, 1.2%, and 1.5% for $P_1=0.12$, 0.06, and 0.04 Torr, respectively.

When the magnetic field was set to 8 G, the run was repeated several times, in order to reduce statistical uncertainties. In these cases, the final TCS's were deduced by averaging the results of each run with the weights of the inverse squares of statistical uncertainties.

Some pairs of different runs partially overlap in their energy region. The comparison of the TCS's in the overlapped energy region is a good probe for a check of the data consistency. It was confirmed that the TCS's were consistent within the statistical uncertainties as far as the strength of magnetic field was identical. Hence the TCS's in the overlaps with same field strength were averaged to obtain the final results. (The differences between two sets of TCS's with different field strength contains some information on forward scattering and spiraling, as will be discussed in Sec. IV.)

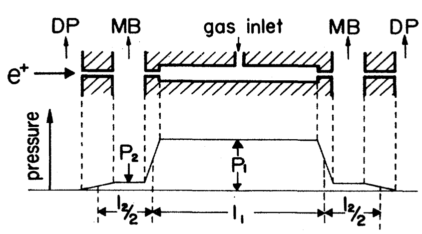

FIG. 4. Assumed pressure distribution for evaluating the integral $\int P(l)dl$. Pressure gradients in the apertures are assumed to be constant (see text). Symbols DP and MB have same definitions as in Fig. 1.

IV. ERRORS

An overall check of energy scale was made by means of the electron resonances as described in Sec. II. It has been shown that no significant error in energy scale exists. The discussion in this section is focused on the errors in TCS's.

A. Pressure distribution

The quoted scale accuracy of the Baratron manometer is 0.08%. Sensor zero drift was found to be within 0.3% of the used pressure throughout each run. The thermal transpiration correction in the present analysis may possibly cause $\pm0.8\%$ to $\pm1.5\%$ systematic errors in TCS, as discussed in Sec. III.

The adopted assumption for the pressure distribution, shown in Fig. 4, gives the exact value for the integral $\int P(l)dl$, provided that the gas flow in each cylindrical aperture is nearly molecular flow so that the pressure gradient at the inside of the aperture is constant, and the discrepancies between the true pressure distribution and the assumed one around the entrance and the exit of each aperture cancel each other by the integration. The former condition is approximately fulfilled in the present experiments, because mean free paths of helium atoms at the pressures used are 1 to 3 mm while the diameter of the apertures is 4 mm. It is not easy, however, to verify the latter condition. We consider here the following conservative case. If the region where the pressure is P_1 extends into the apertures by a depth equal to the aperture diameter, then Eq. (2) causes a 2% overestimate of the TCS. This value may give a reasonable upper limit of the error for the present pressure range.

The validity of the assumed pressure distribution is partially supported by the measurements of TCS's with different pressures (see Fig. 5). Discrepancies between observed TCS's for the different pressures are within statistical uncertainties. Furthermore, there exists no systematic deviation. Therefore the error caused by the uncertainty of the pressure distribution, if any, is only a scale factor which is not affected by a change of pressure setting.

B. Temperature

The drift of gas temperature during each run was within ± 2 K, which results in a $\pm 0.7\%$ error at maximum in the TCS.

C. Beam intensity

The long-term variation of beam intensity, which has been observed mainly during several days after the installation of the moderator in the vacuum chamber, does not significantly affect the ratio n_v/n_g because of the "segmentation" of the measurements. The errors due to statistical fluctuation of the beam intensity, denoted as $\Delta\sigma_{\mathrm{BI}}$, are calculated using

$$\Delta\sigma_{\mathrm{BI}} = \left[\int \rho(l)dl \right]^{-1} \left[\left[\frac{\Delta n_v}{n_v} \right]^2 + \left[\frac{\Delta n_g}{n_g} \right]^2 \right]^{1/2} , \tag{5}$$

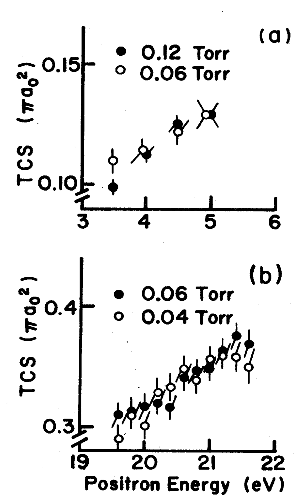

FIG. 5. Pressure dependence of the observed TCS. (a), measured with 3-V acceleration and 13-G magnetic field. (b), measured with 19.5-V acceleration and 8-G magnetic field.

where Δn_v and Δn_g are the statistical errors for the processed data n_v and n_g, respectively.

For the energy-bin width, 0.2 or 0.5 eV, $\Delta\sigma_{\mathrm{BI}}$ are 2—4 % above 3 eV and 4—10% below 3 eV.

D. Forward scattering

When the differential cross sections $d\sigma/d\Omega$ are given, the error in TCS due to incomplete discrimination against forward scattering, denoted as $\Delta\sigma_{\mathrm{FS}}$, can be evaluated from

$$\Delta\sigma_{\mathrm{FS}} = 2\pi \int_0^{\theta_m} \frac{d\sigma}{d\Omega} \sin\theta \, d\theta , \tag{6}$$

where θ_m is the discrimination angle, i.e., the maximum scattering angle of the positrons detected without colliding with the aperture wall. The angle θ_m in the uniform magnetic field can be estimated by the relation

$$\tan\theta_m = \frac{(v_2)_{\max}}{v_1} = \frac{eBR}{mv_1} , \tag{7}$$

where e and m are the positron charge and mass, respectively, and v_1 and v_2 are the axial and transverse components of the velocity of a scattered positron, respectively. v_1 is approximately equal to the incident velocity. The $(v_2)_{\max}$ is the largest v_2 of scattered positrons detected without colliding with the wall, and is related to the product of the magnetic flux density B and the geometrically allowed maximum spiraling radius R for the scattered positrons. The value R depends on the distance between the scattering position and the spectrometer axis, but the reasonable choice of the effective R in the evaluation of $\Delta\sigma_{\mathrm{FS}}$ is given by equating it to one-half the aperture radius (this value gives exact R if all the collisions occur at the axis), which is 1 mm for the present spectrometer.

The errors $\Delta\sigma_{\mathrm{FS}}$ were calculated by the use of Eqs. (6)

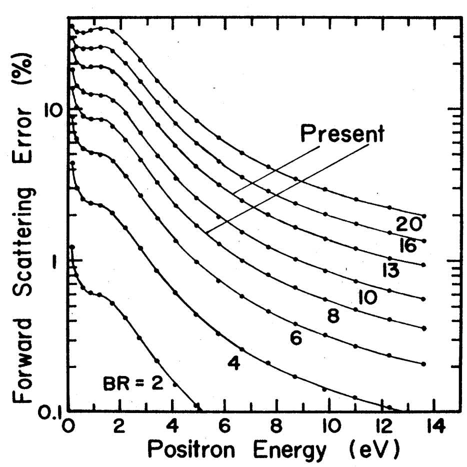

FIG. 6. Forward-scattering errors in TCS as a function of positron energy for different axial-magnetic-field strengths. Calculated from δ_0, δ_1, δ_2, and $\delta_L(3 \leq L \leq 10)$ of Refs. 6, 7, 19, and 20, respectively. The figures by the curves stand for the values of BR (G mm) (see text). For the present spectrometer $R = 1$ mm.

and (7) with a set of theoretical phase shifts, i.e., δ_0 of Campeanu and Humberston[6] (model H14), δ_1 of Humberston and Campeanu[7] (model H5), δ_2 of McEachran *et al.*,[19] and $\delta_L(3 \leqq L \leqq 10)$ of the effective range formula by O'Malley *et al.*[20] The results are shown in Fig. 6. The errors are significantly large below about 3 eV, and rapidly decrease with the increase of energy. These curves are used in Sec. V to compare the present experimental results and the theory.

E. Spiraling of incident positrons

The spiraling of incident positrons due to the axial magnetic field causes two kinds of errors in TCS's. The one is caused by the fact that the spiraling positrons have higher kinetic energies than the energy calculated from the flight time, which should be attributed to nonspiraling, straight-flying positrons. The kinetic energy E of a spiraling positron is expressed as

$$\begin{aligned} E &= E_1 + E_2 , \\ E_1 &= \tfrac{1}{2} m V_1^2 , \\ E_2 &= \tfrac{1}{2} m V_2^2 , \end{aligned} \tag{8}$$

where V_1 and V_2 are the axial and transverse components of the incident positron velocity, respectively. The component V_1 is determined from the flight time, and E_1 is usually identified with the collision energy (as in the present analysis). This causes a systematic error in TCS's because of the existence of E_2, i.e., the observed TCS curve tends to shift toward the lower-energy side. This error will be serious in the case where the true TCS varies rapidly with the increase of energy. The energy shift is approximately equal to the mean value of E_2, denoted as $\langle E_2 \rangle$, and the upper limit of $\langle E_2 \rangle$ can be evaluated by assuming the extreme angular distribution that all the incident positrons are spiraling with the maximum allowed radius R. Thus

$$\langle E_2 \rangle < \frac{(eBR)^2}{2m} . \tag{9}$$

For the present experiments

$$\langle E_2 \rangle < \begin{cases} 0.15 \text{ eV} & \text{for } B = 13 \text{ G} \\ 0.06 \text{ eV} & \text{for } B = 8 \text{ G} . \end{cases}$$

Hence the actual $\langle E_2 \rangle$ is several times smaller than the present energy-bin width, and the error in TCS can be neglected as far as the TCS's presented in this paper are regarded as the mean value over the associated energy bin.

The other error due to the spiraling comes from the fact that the spiraling positrons have a longer flight path in the gas cell than the geometrical gas-cell length. This causes some overestimate of TCS's. We denote this error as $\Delta\sigma_{\text{SP}}$. The ratio of the excess length to the geometrical length is expressed for each positron as

$$\frac{(V_1^2 + V_2^2)^{1/2} - V_1}{V_1} = (1 + E_2/E_1)^{1/2} - 1 . \tag{10}$$

Assuming again the extreme angular distribution for incident positrons, we can deduce the upper limit of the error $\Delta\sigma_{\text{SP}}$ by the use of Eq. (10), as

$$\begin{aligned} \Delta\sigma_{\text{SP}} &\simeq \sigma[(1 + \langle E_2 \rangle / E_1)^{1/2} - 1] \\ &\simeq \sigma \frac{\langle E_2 \rangle}{2E_1} \quad (E_1 \gg \langle E_2 \rangle) , \\ &< \sigma \frac{(eBR)^2}{4mE_1} \\ &\propto \sigma \frac{B^2}{E_1} . \end{aligned} \tag{11}$$

For example, if $E_1 = 2$ eV and $B = 13$ G then the upper limit is 4%. The actual errors $\Delta\sigma_{\text{SP}}$ may be several times smaller than these upper limits.

F. Summary of errors

The statistical errors are dominated by $\Delta\sigma_{\text{BI}}$, which are 2—4 % above 3 eV and amount to 10% at the lowest measured energy 0.6 eV. The other statistical errors, the manometer zero drifts and the temperature drifts, amount to no more than 1%. The systematic errors consist of $\Delta\sigma_{\text{FS}}$, $\Delta\sigma_{\text{SP}}$, and a few-percent scale-factor error due to the uncertainties of the pressure distribution and the thermal transpiration effects. Both $\Delta\sigma_{\text{FS}}$ and $\Delta\sigma_{\text{SP}}$ are significant only in the low-energy region. They partially cancel each other, but the former is several times as large as the latter over the whole energy range.

V. RESULTS AND DISCUSSION

The final results for 8-G and 13-G runs are tabulated in Tables II and III, respectively. The low-energy results around the Ramsauer-Townsend minimum are shown in Fig. 7 with some previous experimental and theoretical results. The present results are in good agreement with those of Wilson[11] (corrected by Sinapius *et al.*[12]) and apparently higher than those of Stein *et al.*[3] except for the energy range below 1 eV. The present TCS's in an 8-G magnetic field are slightly but systematically higher than those in a 13-G field below 2 eV. This means that the forward-scattering discrimination of the former is better than the latter. The comparison of them to the theoretical results of the Kohn variational methods[6,7] was made, taking account of the forward-scattering error $\Delta\sigma_{\text{FS}}$ by the use of the curves in Fig. 6, as shown in Fig. 8. Both of the corrected TCS's are in good agreement with the theoretical curve, except for a few data points in the 13-G data. The fact that both of them agree well with each other is the evidence that the effects of the spiraling of incident positrons, $\Delta\sigma_{\text{SP}}$, is not significant. The systematic behavior of the present results confirms the accuracy of the quoted theoretical results through the simple analysis described above, although the discrimination angle of the present experiments is not so small in this energy range (for example, 10° for 8-G runs at 2 eV and worse below 2 eV) as that of Sinapius *et al.*[12] (7°).

Above about 6 eV, most of the previous experimental results agree within 10% discrepancies[2] at most. The present results in this energy range, therefore, provide an

TABLE II. e^+-He total cross sections with statistical uncertainties measured in an 8-G axial magnetic field. The boundaries of energy bins are listed in the energy columns.

Energy (eV)	TCS (πa_0^2)	Energy (eV)	TCS (πa_0^2)
0.5– 0.7	0.135±0.015	17.1–17.3	0.233±0.006
0.7– 0.9	0.101±0.009	17.3–17.5	0.233±0.006
0.9– 1.1	0.094±0.008	17.5–17.7	0.236±0.006
1.1– 1.3	0.081±0.007	17.7–17.9	0.252±0.006
1.3– 1.5	0.085±0.005	17.9–18.1	0.249±0.006
1.5– 1.7	0.075±0.005	18.1–18.3	0.251±0.006
1.7– 1.9	0.070±0.006	18.3–18.5	0.256±0.006
1.9– 2.1	0.070±0.006	18.5–18.7	0.263±0.006
2.1– 2.3	0.067±0.006	18.7–18.9	0.277±0.007
2.3– 2.5	0.077±0.006	18.9–19.1	0.281±0.007
2.5– 2.7	0.081±0.006	19.1–19.3	0.289±0.007
		19.3–19.5	0.293±0.007
15.1–15.3	0.237±0.007	19.5–19.7	0.300±0.006
15.3–15.5	0.226±0.007	19.7–19.9	0.311±0.006
15.5–15.7	0.223±0.007	19.9–20.1	0.311±0.006
15.7–15.9	0.227±0.007	20.1–20.3	0.320±0.006
15.9–16.1	0.230±0.007	20.3–20.5	0.326±0.006
16.1–16.3	0.225±0.006	20.5–20.7	0.331±0.007
16.3–16.5	0.235±0.006	20.7–20.9	0.344±0.009
16.5–16.7	0.237±0.006	20.9–21.1	0.353±0.009
16.7–16.9	0.233±0.005	21.1–21.3	0.362±0.009
16.9–17.1	0.234±0.005	21.3–21.5	0.368±0.009
		21.5–21.7	0.362±0.010

overall check of our spectrometer and methods. The TCS's from about 7 to 17 eV are in agreement with those of Stein *et al.*[3] within few-percent differences, although the present ones are systematically higher (see Fig. 9). The theoretical curves are deduced by using δ_0 and δ_1 of Refs. 6 and 7, respectively, δ_2 of two different authors,[19,20] and the higher-partial-wave phase shifts of O'Malley *et al.*[20] In the higher-energy region of the fig-

TABLE III. e^+-He total cross sections with statistical uncertainties measured in a 13-G axial magnetic field. The boundaries of energy bins are listed in the energy columns.

Energy (eV)	TCS (πa_0^2)	Energy (eV)	TCS (πa_0^2)
0.5–0.7	0.127±0.008	10.25–10.75	0.203±0.008
0.7–0.9	0.090±0.007	10.75–11.25	0.202±0.007
0.9–1.1	0.085±0.006	11.25–11.75	0.213±0.007
1.1–1.3	0.076±0.005	11.75–12.25	0.213±0.007
1.3–1.5	0.067±0.004		
1.5–1.7	0.063±0.004	13.25–13.75	0.219±0.006
1.7–1.9	0.066±0.004	13.75–14.25	0.224±0.006
1.9–2.1	0.070±0.004	14.25–14.75	0.221±0.006
2.1–2.3	0.067±0.004	14.75–15.25	0.228±0.006
2.3–2.5	0.081±0.005	15.25–15.75	0.233±0.006
2.5–2.7	0.079±0.004	15.75–16.25	0.229±0.006
2.7–2.9	0.077±0.004	16.25–16.75	0.229±0.005
2.9–3.1	0.083±0.005	16.75–17.25	0.232±0.005
		17.25–17.75	0.246±0.007
3.25–3.75	0.102±0.003	17.75–18.25	0.245±0.006
3.75–4.25	0.113±0.003	18.25–18.75	0.263±0.006
4.25–4.75	0.121±0.003	18.75–19.25	0.276±0.006
4.75–5.25	0.126±0.004	19.25–19.75	0.293±0.007
5.25–5.75	0.137±0.005	19.75–20.25	0.319±0.008
5.75–6.25	0.147±0.005	20.25–20.75	0.326±0.007
		20.75–21.25	0.365±0.008
7.25–7.75	0.166±0.006	21.25–21.75	0.375±0.008
7.75–8.25	0.173±0.006	21.75–22.25	0.391±0.009
8.25–8.75	0.181±0.006		
8.75–9.25	0.188±0.006		

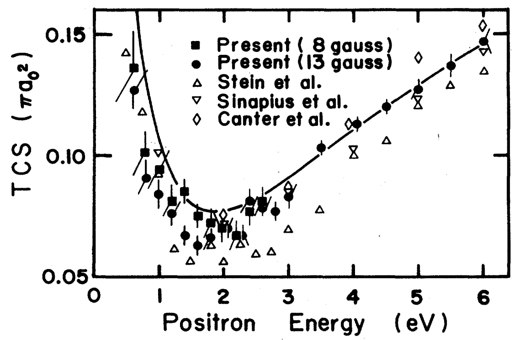

FIG. 7. Present results for positron-helium total cross sections around the Ramsauer-Townsend minimum. The closed symbols are the present results. The quoted experimental results are from Refs. 3 (△), 12 (▽), and 4 (◇). The solid curve represents the theoretical results calculated from δ_0, δ_1, and $\delta_L(2 \leq L)$ of Refs. 6, 7, and 20, respectively. The error bars represent statistical uncertainties only.

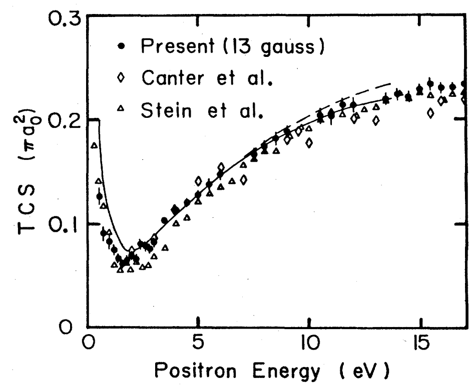

FIG. 9. Present results for positron-helium total cross sections below the Ps-formation threshold. The quoted experimental results are from Refs. 3 (△) and 4 (◇). The solid curve is obtained by using δ_0, δ_1, δ_2, and $\delta_L(3 \leq L)$ of Refs. 6, 7, 19, and 20, respectively. The dashed curve is obtained by using δ_0, δ_1, and $\delta_L(2 \leq L)$ of Refs. 6, 7, and 20, respectively. The error bars represent statistical uncertainties only.

ure, the choice of d-wave phase shifts causes considerable difference among the resultant TCS's. The TCS using O'Malley's δ_2 (dashed curve) is 6% higher than that using McEachran's[19] (solid curve) at 13.6 eV. Drachman's[21] δ_2 gives slightly larger TCS's (not drawn for clarity) than McEachran's (2% at 13.6 eV), but both results run through the center of the narrow band within which the present results are distributed. The TCS at 13.6 eV using δ_2 of Amusia *et al.*[22] is 3% higher than that using McEachran's. At the energies around 10 eV the present experimental errors are dominated by the statistical errors and a few-percent scale-factor error due to the uncertainty of the pressure distribution in the gas cell. The latter never amounts to 6% and seems to cause overestimates of TCS's. Thus it can be concluded that the use of Drachman's or of McEachran's δ_2 provides better results than does use of O'Malley's or Amusia's. With this choice for d wave, the agreement between the present experimental results and the theory is strikingly good as seen in Fig. 9.

The results around the Ps-formation threshold are shown in Fig. 10. The two sets of the present results in the different strengths of magnetic field agree well within the statistical uncertainties, as expected, since the effects of the incomplete discrimination against forward scattering and the spiraling may be very small in this energy range. They are also in general agreement with the previous experimental results, though the present ones are systematically high. The well-known change of the slope at the Ps-formation threshold is clearly seen, especially in the 8-G results. The bend is located at 17.7 eV, which agrees with the exact threshold 17.8 eV within the accuracy of the energy scale.

In conclusion, the present results in the higher-energy region are in general agreement with the previous experi-

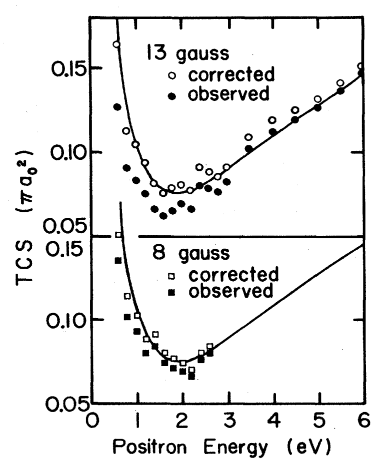

FIG. 8. Comparison of the theoretical results and the present results with and without correction for the forward-scattering errors. Both theoretical curves are the same as that of Fig. 7.

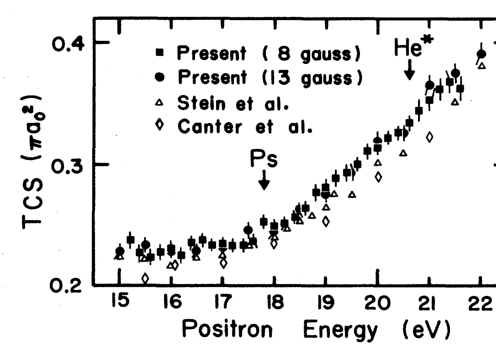

FIG. 10. Present results for positron-helium total cross sections around the Ps-formation threshold. The quoted experimental results are from Refs. 3 (△) and 4 (◇). The arrows indicate the thresholds of positronium formation and the excitation of the 2^1S state of the helium atom. The error bars represent statistical uncertainties only.

mental results and in excellent agreement with the theory for the elastic scattering. This agreement also means that the present spectrometer and methods do not contain any significant systematic errors other than the forward scattering and the spiraling, and provides evidence for the reliability of the present lower-energy results. In the vicinity of the Ramsauer-Townsend minimum, there has remained a slight discrepancy between the present results and the theory, but it has been fully explained by the incomplete discrimination against forward scattering evaluated in a simple and straightforward way. Thus we can conclude that the reasonable consistency between the present experiments and the theory has been found over the whole energy range below the Ps-formation threshold. A similar consistency with the theory has been demonstrated[8,9] for the measurements of Stein *et al.* when incomplete discrimination against forward scattering is taken into account.

For higher-precision measurements of positron-helium TCS's, a much higher-intensity slow positron beam will be required as well as better energy resolution, and it will enable us to investigate finer structure of TCS's, such as resonances, which we did not thoroughly investigate because of the weakness of the incident beam.

ACKNOWLEDGMENTS

The authors wish to thank the staffs of the Laboratory of Nuclear Radiation of the Institute for Chemical Research and Radioisotope Research Center, Kyoto University, for their valuable help during the lengthy course of this work. This work was supported in part by a Grant-in-Aid for Scientific Research of the Japanese Ministry of Education.

---

*Present address: Research Center for Nuclear Physics, Osaka University, Ibaragi, Osaka 567, Japan.

[1]D. G. Costello, D. E. Groce, D. F. Herring, and J. Wm. McGowan, Can. J. Phys. **50**, 23 (1972).

[2]A comprehensive review on the subject is given in W. E. Kauppila and T. S. Stein, Can. J. Phys. **60**, 471 (1982).

[3]T. S. Stein, W. E. Kauppila, V. Pol, J. H. Smart, and G. Jesion, Phys. Rev. A **17**, 1600 (1978).

[4]K. F. Canter, P. G. Coleman, T. C. Griffith, and G. R. Heyland, J. Phys. B **6**, L201 (1973).

[5]J. R. Burciaga, P. G. Coleman, L. M. Diana, and J. D. McNutt, J. Phys. B **10**, L569 (1977).

[6]R. I. Campeanu and J. W. Humberston, J. Phys. B **10**, L153 (1977).

[7]J. W. Humberston and R. I. Campeanu, J. Phys. B **13**, 4907 (1980).

[8]J. M. Wadehra, T. S. Stein, and W. E. Kauppila, J. Phys. B **14**, L783 (1981).

[9]T. S. Stein and W. E. Kauppila, Adv. At. Mol. Phys. **18**, 53 (1982).

[10]J. W. Humberston, J. Phys. B **11**, L343 (1978).

[11]W. G. Wilson, J. Phys. B **11**, L629 (1978).

[12]G. Sinapius, W. Raith, and W. G. Wilson, J. Phys. B **13**, 4079 (1980).

[13]G. E. Lee-Whiting, Atomic Energy of Canada, Limited (Chalk River) Report No. CRT-673 (unpublished).

[14]R. E. Kennerly, Phys. Rev. A **21**, 1876 (1980).

[15]S. Cvejanovic and F. H. Read, J. Phys. B **7**, 1180 (1974).

[16]P. G. Coleman, T. C. Griffith, and G. R. Heyland, Appl. Phys. **5**, 223 (1974).

[17]T. Edmonds and J. P. Hobson, J. Vac. Sci. Technol. **2**, 182 (1965).

[18]G. C. Baldwin and M. R. Gaerttner, J. Vac. Sci. Technol. **10**, 215 (1973).

[19]R. P. McEachran, D. L. Morgan, A. G. Ryman, and A. D. Stauffer, J. Phys. B **10**, 663 (1977); corrigendum, *ibid.* **11**, 951 (1978).

[20]T. F. O'Malley, L. Rosenberg, and L. Spruch, Phys. Rev. **125**, 1300 (1962).

[21]R. J. Drachman, Phys. Rev. **144**, 25 (1966).

[22]M. Ya. Amusia, N. A. Cherepkov, L. V. Chernysheva, and S. G. Shapiro, J. Phys. B **9**, L531 (1976).